

Low Mass WIMP Searches with a Neutrino Experiment: A Proposal for Further MiniBooNE Running

Presented to the FNAL PAC Oct 15, 2012

The MiniBooNE Collaboration

R. Dharmapalan, S. Habib, C. Jiang, & I. Stancu
University of Alabama, Tuscaloosa, AL 35487

R. A. Johnson & D.A. Wickremasinghe
University of Cincinnati, Cincinnati, OH 45221

F.G. Garcia , R. Ford, T. Kobilarcik, W. Marsh,
C. D. Moore, D. Perevalov, & C. C. Polly
Fermi National Accelerator Laboratory, Batavia, IL 60510

J. Grange & H. Ray
University of Florida, Gainesville, FL 32611

R. Cooper & R. Tayloe
Indiana University, Bloomington, IN 47405

G. T. Garvey, W. Huelsnitz, W. Ketchum, W. C. Louis, G. B. Mills,
J. Mirabal, Z. Pavlovic, & R. Van de Water,
Los Alamos National Laboratory, Los Alamos, NM 87545

B. P. Roe
University of Michigan, Ann Arbor, MI 48109

A. A. Aguilar-Arevalo
Instituto de Ciencias Nucleares, Universidad Nacional Autónoma de México, D.F. México

P. Nienaber
Saint Mary's University of Minnesota, Winona, MN 55987

The Theory Collaboration

B. Batell
University of Chicago, Chicago, IL, 60637

P. deNiverville , D. McKeen, M. Pospelov, & A. Ritz
University of Victoria, Victoria, BC, V8P 5C2

Contents

1	Executive Summary	3
2	Introduction and Motivation	4
3	Theoretical Scenario	6
3.1	Light WIMPs and Dark Forces	6
3.2	Light WIMP Production at MiniBooNE	6
4	MiniBooNE WIMP Detection Strategy and Sensitivities	8
4.1	Reducing Backgrounds from Neutrinos	8
4.2	WIMP Signal Extraction	11
4.2.1	WIMP Sensitivities with NC Nucleon data set	12
4.2.2	WIMP Sensitivities with NC Electron data set	14
4.2.3	Using Timing to Enhance Wimp Sensitivity	15
4.3	Sensitivity Plots and Signal Significance	18
4.4	Analysis Improvements	19
5	Timing and Beam Targeting Improvements	22
6	Deploying the 25m Absorber	22
7	Logistics of the Extended Run	23
8	Summary	25
9	The Request	25

1 Executive Summary

The MiniBooNE experiment at the Fermi National Accelerator Laboratory (FNAL) was designed to search for neutrino oscillations at the LSND mass scale. Running since 2002 in both neutrino and antineutrino mode, MiniBooNE has successfully accomplished these primary goals and produced evidence that supports the claims of LSND oscillations. As a single-detector oscillation experiment, its systematic uncertainties now nearly dominate the total measurement error, and therefore more statistics in either neutrino or antineutrino mode will not add significant new information to the question of oscillations.

A new opportunity to exploit the specific features of the MiniBooNE configuration arises from the physics of certain particle dark matter candidates. Recent theoretical work has highlighted that sub-GeV weakly interacting massive particles (WIMPs) can be interesting and viable candidates for dark matter in the Universe, but fall into a mass range that is difficult to probe using direct searches. The MiniBooNE experiment was designed to produce a significant flux of neutrinos using a large number of protons impacting a Beryllium target, and then detecting them with a large volume electromagnetically-sensitive detector at short distance (~ 500 m). It turns out that with some tweaking of the beam configuration, i.e. steering the proton beam past the target and deploying the 25m absorber, this is an ideal setup to search for low mass (< 200 MeV) WIMPs in a parameter region that is consistent with the required thermal relic abundance, and moreover which overlaps the region in which these models can resolve the muon $g - 2$ discrepancy.

MiniBooNE has completed its antineutrino run, and has the capability for continued stable operation for many years. The remaining collaboration is committed to running the experiment and analyzing the data in a timely manner. With the proton on target (POT) rates achieved before the shutdown, and assuming no technical problems, MiniBooNE can reach the requested 2×10^{20} POT run goal by early 2014 when MicroBooNE begins operation and switches to neutrino mode.

Using MiniBooNE to search for low mass WIMP dark matter would take a well understood neutrino experiment and put it to a new and exciting use. Confirming light mass WIMPs would be a huge discovery with implications for particle physics and cosmology. In addition, a successful execution of this proposal and a demonstration of the technique to measure light mass WIMPs with fixed target proton accelerators would allow future dedicated experiments to be proposed with the current suite of FNAL proton accelerators and Project X.

MiniBooNE requests running to collect a total of 2.0×10^{20} POT in beam off target mode and with the 25m absorber deployed. This will allow a powerful search for low mass WIMPs in a parameter region consistent with the required cosmic relic density, and in which these models can resolve the muon $g - 2$ discrepancy. The experiment further requests that this beam be delivered in FY2013 and 2014 before the MicroBooNE experiment turns on.

2 Introduction and Motivation

The MiniBooNE experiment was designed to test the neutrino oscillation interpretation of the LSND signal [1] in both neutrino and antineutrino modes. MiniBooNE has successfully completed this program with 6.5×10^{20} POT in neutrino mode and 11.3×10^{20} POT in antineutrino mode [2], resulting in a combined 3.8σ excess of electron like events. It has become apparent that the time required to gain enough statistics to make a meaningful improvement in significance is on the order of many years. Because of this limitation, it was decided to pursue new systematically different approaches to understand the oscillation signal. This is the subject of an LOI that was submitted concurrently with this proposal. The LOI describes the addition of scintillator to the detector to make systematically measurable changes to the oscillation signal. Before this is done, however, a new opportunity has arisen to explore the physics of dark matter that requires the current detector configuration.

The case for the existence of dark matter is strong, with evidence coming from a variety of observations in astrophysics and cosmology. Indeed, the existence of dark matter provides one of the strongest motivations for physics beyond the standard model, and a large experimental program to detect non-gravitational interactions of dark matter has been pursued over the past two decades. Underground direct detection experiments searching for the recoil signal of weakly interacting massive particles (WIMPs) scattering off nuclei lose sensitivity if the WIMP mass is below a few GeV. It has recently been suggested [3, 4, 5] that several on-going neutrino beam experiments, and MiniBooNE in particular, could be sensitive to sub-GeV WIMP particles due to the large number of protons on target (POT) and by virtue of the large detector mass.¹ The following proposal summarizes this idea and outlines how MiniBooNE can achieve a unique and interesting search for light WIMPs.

Light WIMPs of a few MeV mass were originally proposed [9] as candidates to explain (via annihilation) a strong diffuse 511 keV emission from the galactic bulge, that may require a new physics contribution on top of the identified astrophysical components [10]. A crucial ingredient of realistic light WIMP models (below the lower end of the so-called Lee-Weinberg mass window for WIMPs [11]) is the presence of light GeV-scale or sub-GeV *mediator* particles that couple both to the standard model fields and to WIMPs [12, 13, 14] (see also [15]). Light mediators are necessary to open up a new annihilation channel in the early universe for sub-GeV WIMPs to achieve the required relic abundance via thermal freeze-out. This scenario provides a new approach to search for dark matter at neutrino experiments such as MiniBooNE: the light mediator particles will be produced copiously in the primary proton-target collisions and subsequently decay to dark matter particles, thus yielding a relativistic dark matter beam which can be detected through elastic scattering on nuclei or electrons in the near detector. Vector or scalar mediators up to a few 100 MeV mass have been under intense experimental scrutiny in the past few years, partly because they also provide one of the most economical ways of reconciling the discrepancy in measured and calculated values of $g - 2$ of the muon [16, 17]. Therefore, both light WIMPs and light mediators are of considerable interest as possible explanations for various puzzles in both astrophysics and particle physics. In a related direction, the search for GeV and sub-GeV mediators (or “dark forces”) has become a mainstay of searches for new physics at the intensity frontier [18, 19]

¹See [6, 7, 8] for other recent approaches to the detection of light dark matter.

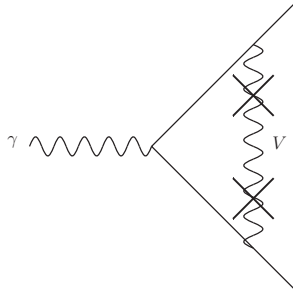


Figure 1: The contribution to the anomalous magnetic moment of SM fermions from the vector mediator. The crosses represent the kinetic mixing κ of the vector V with the photon.

(see also [20] and references therein).

Improved sensitivity to WIMP interactions is achieved by taking advantage of the fact that the MiniBooNE beamline can be easily run in a mode where the 8.9 GeV proton beam is steered off target. The protons subsequently travel the length of the decay pipe through air and impact the deployed 25m absorber. In this configuration, the neutrino flux can be reduced by two orders of magnitude, while the WIMP production mechanism remains unaffected. This simple technique significantly reduces neutrino backgrounds that can mimic the interaction of WIMPs via neutral current like scattering off nucleons or electrons.

One unique advantage that MiniBooNE has in this search is the ability to rely on the work done over the last 10 years in understanding the detector response and the standard backgrounds – such as those coming from the dirt surrounding the detector or cosmic rays. We have a robust and well-tested particle identification tool-set which will be used in the present analysis. MiniBooNE has also reported a number of high-statistics neutrino cross section measurements in both the neutral current and charged current channels [21, 22, 23, 24, 25, 26, 27, 28]. Altogether, the experiment has measured the cross sections for 90% of the neutrino interactions in MiniBooNE. A new dark matter search experiment would have to spend years in order to achieve a similar understanding of the detector and the backgrounds.

The region in WIMP/mediator parameter space (mass and cross section) that can be covered is at low mass from 10 MeV up to 200 MeV, where other experiments have reduced sensitivity, and where indirect probes (muon $g - 2$) currently provide the best constraints. This is a unique measurement that MiniBooNE can make with only a year’s worth of data that will allow it to play an important role in the future FNAL program that involves muon $g - 2$ and WIMP searches in general. If this proposal proves successful in execution, it can also lead to further dedicated WIMP search experiments using a better designed beam dump and a spatially and temporally high resolution scintillator fiber detector. This experiment would use protons from one of the the current suite of FNAL accelerators, or Project X, where the search could be significantly extended in mass and cross section.

3 Theoretical Scenario

3.1 Light WIMPs and Dark Forces

Minimal sub-GeV WIMP scenarios are characterized by the mass scale and interaction strengths of the WIMP itself and the mediator that controls the coupling to the Standard Model. General dictates of effective field theory would suggest that the leading interactions of a singlet mediator will be through renormalizable interactions, of which only three are available in the Standard Model. Thus it is possible to be fairly systematic in exploring the constraints on the various WIMP–mediator combinations. In practice, models of sub-GeV dark matter are subject to a number of cosmological, astrophysical, and particle physics constraints, as discussed *e.g.* in [4, 5]. These constraints select out a massive U(1) vector V^μ as the most viable mediator candidate, coupling via kinetic mixing with the hypercharge gauge boson [29], and leading below the weak scale to kinetic mixing with the photon, $\mathcal{L}_{\text{mix}} = \frac{\kappa}{2} F_{\mu\nu} V^{\mu\nu}$. Moreover, light dark matter is strongly constrained by the impact of annihilation in the late universe, in particular on the CMB, and thus viable WIMP candidates should exhibit p -wave annihilation in low-velocity regimes. This singles out a complex scalar WIMP χ charged under the new U(1) vector as a natural light dark matter candidate. Therefore, the benchmark model we consider takes the form [4, 5],

$$\mathcal{L}_{\text{DM}} = V_\mu (e\kappa J_{\text{em}}^\mu + e' J_\chi^\mu) + \mathcal{L}_{\text{kin}}(V, \chi) + \dots \quad (1)$$

on using $\partial_\mu F^{\mu\nu} = eJ_{\text{em}}^\nu$, with the electromagnetic current $J_{\text{em}}^\mu = Q_f \bar{f} \gamma^\mu f + \dots$, to rewrite the kinetic mixing interaction, $\frac{\kappa}{2} F_{\mu\nu} V^{\mu\nu}$. $J_\chi^\mu = i(\chi^\dagger \partial^\mu \chi - \partial^\mu \chi^\dagger \chi) + \mathcal{O}(V^\mu)$ is the corresponding U(1) current for scalar dark matter, with gauge coupling $e' \equiv \sqrt{4\pi\alpha'}$. In what follows, we assume small mixing κ , perturbative $\alpha' \sim \alpha$, and that $m_V > 2m_\chi$. The latter assumption determines the mass hierarchy of interest here, ensuring that $V \rightarrow 2\chi$ is the dominant decay mode of the vector. Requiring that the dark matter candidate is a WIMP (i.e. with its relic abundance fixed to the measured value via thermal freeze-out²), provides one constraint on the four parameters of the model $\{m_\chi, m_V, \kappa, \text{ and } \alpha'\}$. This light WIMP model has been motivated above on general grounds. Although various modifications of this framework are plausible, this particular model is rather unique as a minimalist extension of the Standard Model, and in its ability to escape a number of particle physics and astrophysics constraints. In addition, the light kinetically mixed vector that serves as a mediator in this model also gives a contribution to the anomalous magnetic moments of SM fermions, as seen in Fig. 1, and can explain the current discrepancy in the muon $g - 2$ [16, 17].

3.2 Light WIMP Production at MiniBooNE

At proton fixed-target experiments, there are two primary production modes for χ , where we assume $m_V > 2m_\chi$ so that (for $\alpha' \sim \alpha$ and small mixing κ) the on-shell decay $V \rightarrow 2\chi$ has the dominant branching fraction. The first involves direct parton-level processes such as

²Thermal freeze-out via the annihilation $\chi\chi \rightarrow V^* \rightarrow \text{SM states}$ is viable for $m_\chi < m_V$. For larger (sub-GeV) WIMP masses, the dominant annihilation is through $\chi\chi \rightarrow VV$ which has too large a cross section and can cause problems with the CMB.

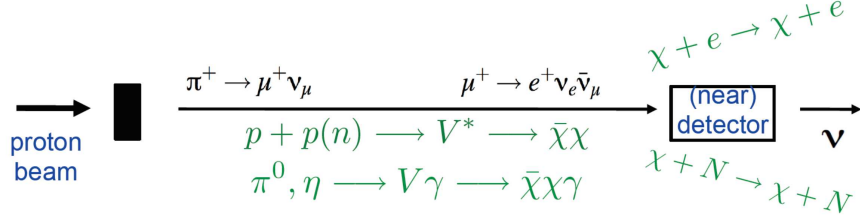


Figure 2: An illustration of the dark matter production modes and elastic scattering signatures.

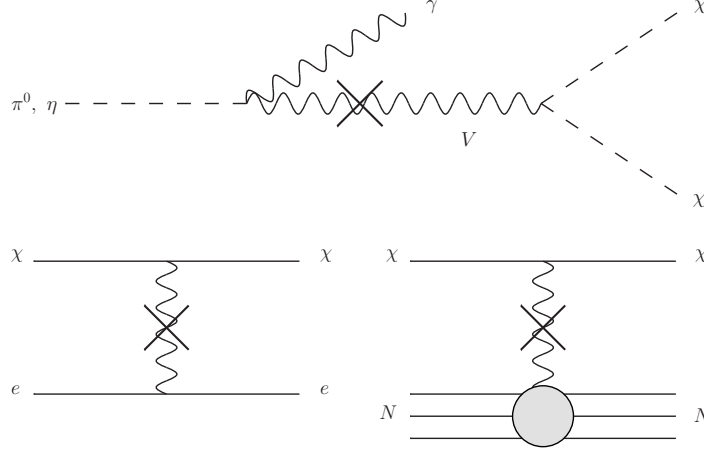


Figure 3: Top: The production of a WIMP pair through neutral meson decay. Bottom: The scattering of a WIMP in the MiniBooNE detector. The cross again represents the kinetic mixing between the vector mediator V and the photon.

$p + p(n) \rightarrow V^* \rightarrow \chi^\dagger \chi$. The second is through decays of mesons with large radiative branching such as π^0 and η in the form $\pi^0, \eta \rightarrow V\gamma \rightarrow \chi^\dagger \chi\gamma$. Once produced, the dark matter beam can be detected via elastic scattering on nucleons or electrons in the detector, as the signature is similar to the neutral current scattering of neutrinos. The basic production and detection principle is summarized in Fig. 2.

At MiniBooNE, the most relevant production mechanisms are via π^0 and η which subsequently decay to vectors that in turn decay to WIMPs. These WIMPs can then scatter on the nuclei or electrons in the MiniBooNE detector. This process is detailed in Fig. 3. We estimate the π^0 and η production by averaging and scaling [5] the π^+ and π^- Sanford-Wang distributions used in Ref. [30] and use the cuts from the analysis of neutral current scattering (on nucleons) in Ref. [30] to obtain a total efficiency of about 35%. (Similar efficiencies were adopted in analyzing electron scattering.) Contours in the parameter space of the model were computed corresponding to 1, 10, and 1000 neutral current-like scattering events on nucleons or electrons with 2×10^{20} POT at MiniBooNE. While the Sanford-Wang distribution used corresponds to a beryllium target, the results are not expected to differ much when steering the beam into the iron beam dump since the ratio of the charged hadron production (which sets the number of neutrinos produced) to neutral hadrons (which sets the number of WIMPs produced) does not strongly depend on atomic number.

In Fig. 4, these contours are shown in the plane of direct-detection scattering cross

section σ_N vs dark matter mass m_χ for $m_V = 300$ MeV and $\alpha' = \alpha$. This cross-section, corresponding to the regime of coherent scattering on nuclei, has different kinematics from the actual scattering cross-section at MiniBooNE. However, it allows the MiniBooNE sensitivity to be compared to direct detection experiments, whose sensitivity weakens considerably at low mass (we show the best limits from CRESST [31] and XENON10 [32]). We also exhibit the existing particle physics constraints on the parameter space. Note the interesting region where the band in which the $(g - 2)_\mu$ discrepancy is alleviated coincides with the required relic density and with a potentially sizable number of events at MiniBooNE. Comparison with a number of existing exclusion regions and ongoing searches in the “dark force” scenario [18, 19, 20], where the light vector instead decays dominantly to the Standard Model, is aided by considering the κ vs m_V plane for fixed dark matter mass. This parameter space is shown in Fig. 5, for the two regimes that we can alternately characterize as ‘dark’, with $m_V > 2m_\chi$ so that V decays invisibly, and ‘visible’ with $m_V < 2m_\chi$ so that V decays to light SM degrees of freedom. The dominant invisible branching of the vector to dark matter weakens or removes many of the existing limits (see Fig. 5 for further details). In Fig. 6, the MiniBooNE sensitivity contours are shown in the κ vs m_V plane for $m_\chi = 10$ MeV and $\alpha' = \alpha$. Note once again the interesting coincidence between the region of parameter space that MiniBooNE is sensitive to as well as those that solve the $(g - 2)_\mu$ discrepancy and give the required relic density.

The masses chosen above are representative in that the WIMP production at MiniBooNE is not strongly sensitive to choices of mass so long as the mediator can be produced in the decays of light mesons, $m_V < m_\eta$, and it decays invisibly, i.e. $m_V > 2m_\chi$. Moreover, while the potential MiniBooNE sensitivity is illustrated here for the model of light scalar WIMPs and a vector mediator, the experimental results obtained in such a study could easily be translated to consider the sensitivity to other types of mediators and hidden sector particles within the same kinematic range. This would allow a comprehensive coverage of many viable light WIMP models, and explore the region of interest for mediator masses and couplings relevant in connection with the muon $g - 2$ discrepancy.

4 MiniBooNE WIMP Detection Strategy and Sensitivities

4.1 Reducing Backgrounds from Neutrinos

WIMP signals in the MiniBooNE detector look like neutral current scattering events off nucleons or electrons, and the largest source of backgrounds to this process will be neutral current neutrino interactions. The number of background events are in the tens of thousands, and would make searches for WIMP signals extremely difficult. A method is proposed that will reduce the neutrino flux by up to two orders of magnitude, making sensitive searches achievable.

The neutrino flux can be significantly reduced by pointing the beam past the target where it then travels through air to the 50m iron absorber, or 25m iron absorber if deployed. There is a 1 cm air gap around the target between the Be and the inner horn conductor. Since the beam spot is 1 mm in size, there is ample room to safely point the beam past the target.

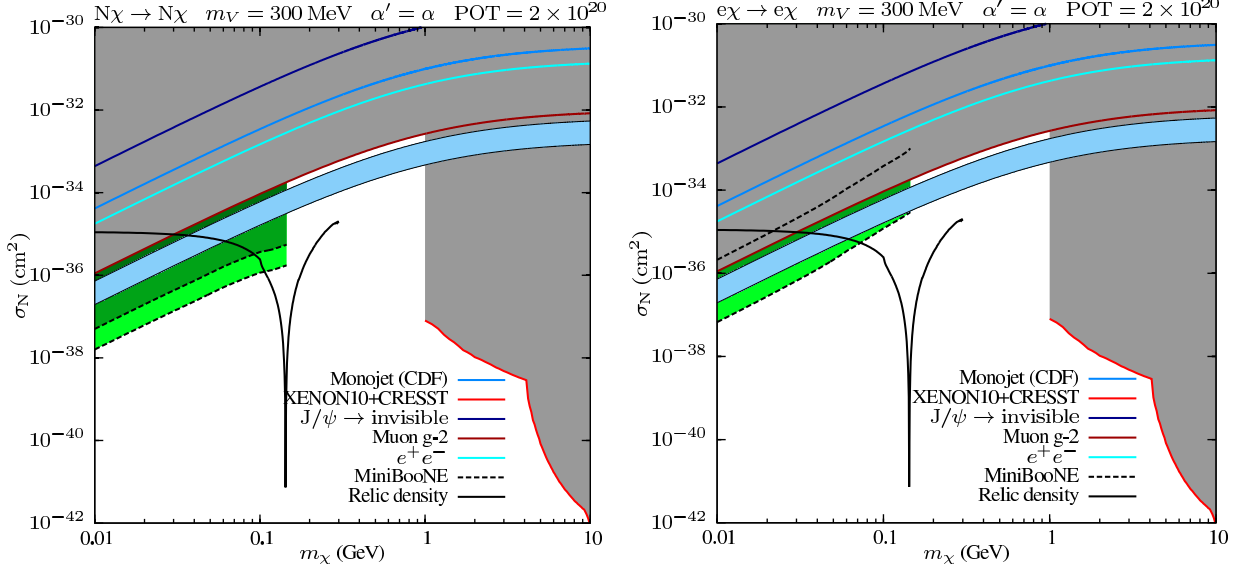


Figure 4: Regions of nucleon-WIMP scattering cross section (corresponding to dark matter in the halo moving with $v \sim 10^{-3}c$) vs WIMP mass. The plot uses $m_V = 300$ MeV and $\alpha' = \alpha$. Constraints are shown from dark force searches (labeled e^+e^- , and including from left-to-right limits from KLOE, APEX, MAMI and BaBar [20], limits on $pp \rightarrow j + \text{inv.}$ [33] (labeled Monojet), limits on $J/\psi \rightarrow \text{inv. decays}$ [34], excessive contributions to $(g-2)_\mu$ [17], together with low-mass limits from the direct detection experiments CRESST [31] (1-4 GeV) and XENON10 [32] (4-10 GeV). Note that a similar, but slightly stronger, exclusion contour to CRESST has also been obtained by DAMIC [35]. The light blue band indicates the region where the current $\sim 3\sigma$ discrepancy in $(g-2)_\mu$ is alleviated by 1-loop corrections from the vector mediator [17]. The solid black line shows points where the present relic density of the WIMP matches observations—the structure in this occurs when the WIMP mass is such that its annihilation during freeze-out through an off-shell s -channel V^* is resonantly enhanced. This relationship only applies for $m_\chi < m_V$. The left panel shows regions where we expect 1–10 (light green), 10–1000 (green), and more than 1000 (dark green) elastic scattering events off nucleons in the MiniBooNE detector with 2×10^{20} POT. The right panel shows the same for elastic scattering off electrons.

The interaction length for 8.9 GeV protons in air at atmospheric pressure is about 1 km, so that 50m is about a 5% interaction length.

When the protons impact the iron absorber, the charged mesons quickly range out in the dense iron and are absorbed, thereby preventing the decay that produces neutrinos. The few charged mesons that are produced in the air or in the iron absorber and decay are not focused and hence the neutrinos do not gain from the horn focusing, again reducing the flux at the detector. Monte Carlo simulations show in Figure 7 the flux reduction relative to normal neutrino mode running. Integrating the flux reduction over all energies, one obtains the Monte Carlo prediction for the flux ratio:

$$\frac{\text{Flux (events/POT)}^{\nu \text{ mode}}}{\text{Flux (events/POT)}^{\text{beam-off-target mode}}} = 36. \quad (2)$$

In March of 2012 a successful one week run with the beam pointed off target onto the 50m dump collected 5.5×10^{18} POT. With this data set the muon neutrinos were reconstructed and the following rate reduction was measured:

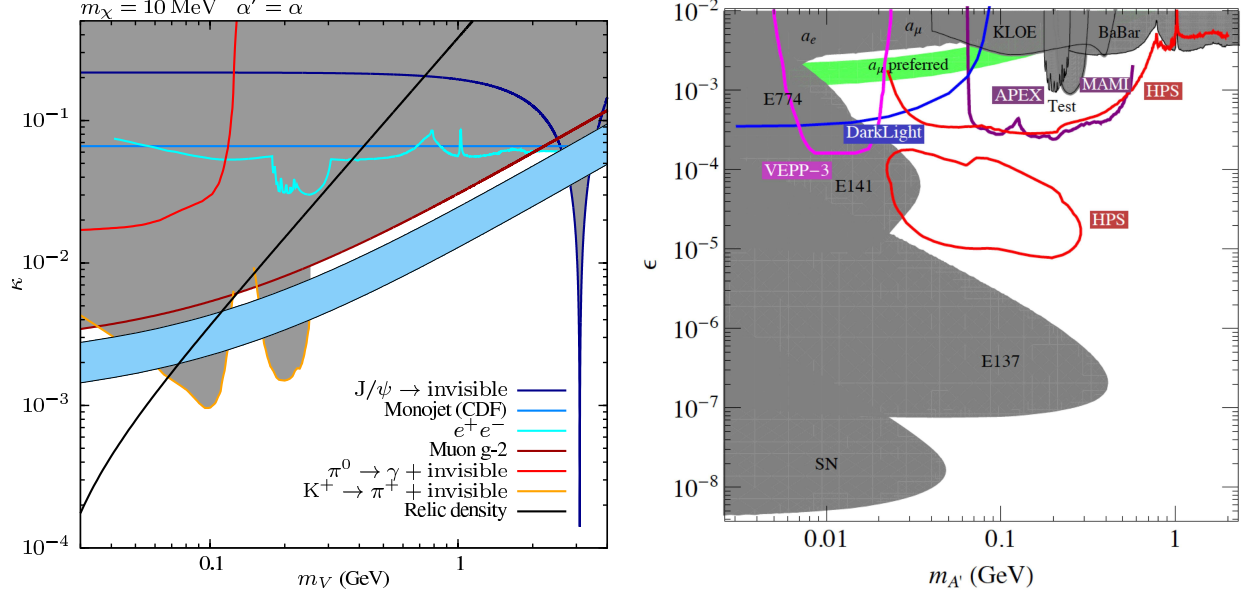


Figure 5: Regions of mixing angle κ (ϵ) vs vector mass m_V ($m_{A'}$), contrasting the existing sensitivity to light vectors in the two scenarios where the dominant decay mode of the vector is either visible or invisible. On the left we show the sensitivity to the light dark matter model considered here, in which $m_V > 2m_\chi$ so that the vector predominantly decays invisibly and $\text{Br}(V \rightarrow \text{SM}) \sim \kappa^2 \alpha' / \alpha$ with $\alpha' = \alpha$. On the right (reproduced from [20], figure courtesy of R. Essig), this is contrasted with the sensitivity in the absence of light dark matter, or with $m_V < 2m_\chi$, so that $\text{Br}(V \rightarrow \text{SM}) \sim \mathcal{O}(1)$. The shaded regions are existing limits, while the open contours are current and planned searches. Note that in the light dark matter scenario, many of the existing dark force constraints shown on the right are weakened by the reduced leptonic branching ratio, while beam dump limits that rely on a long lifetime for the V are removed entirely. In the left-hand plot, as in Fig. 4, constraints from dark force searches (labeled e^+e^-) [20], $pp \rightarrow j + \text{inv.}$ [33] (labeled Monojet), $J/\psi \rightarrow \text{inv.}$ decays [34], and excessive contributions to $(g-2)_\mu$ [17] are shown, along with limits from $\pi^0 \rightarrow \gamma + \text{inv.}$ [36] and $K^+ \rightarrow \pi^+ + \text{inv.}$ [37] decays. The light blue band again indicates the region where the current $\sim 3\sigma$ discrepancy in $(g-2)_\mu$ is alleviated [17], and the solid black line shows the parameters required to reproduce the observed relic density of dark matter.

$$\frac{\text{Rate}(\text{events/POT})^{\nu \text{ mode}}}{\text{Rate}(\text{events/POT})^{\text{beam-off-target mode}}} = 42 \pm 7. \quad (3)$$

The Monte Carlo flux reduction ratio is close to the measured rate reduction value. However, differences are expected as the flux ratio does not include the effects of cross sections and detection efficiency, which the rate measurement includes. Figure 8 shows various event kinematics for reconstructed muon neutrino events from the beam off target running, and the Monte Carlo is relatively normalized. The various kinematic distributions look normal relative to the Monte Carlo.

When determining neutrino background rates for beam off target running, we will use the measured rate value of 42 reduction with respect to neutrino mode. By deploying the 25m absorber, the flux reduction is increased by a further factor of two as shown in Figure 7. This is to be expected since most of the neutrino production is from proton interactions in air. If we reduce the path length in air by a factor of two ($50\text{m}/25\text{m}$), then the neutrino rate is reduced by the same factor. This extra neutrino reduction is important for improving

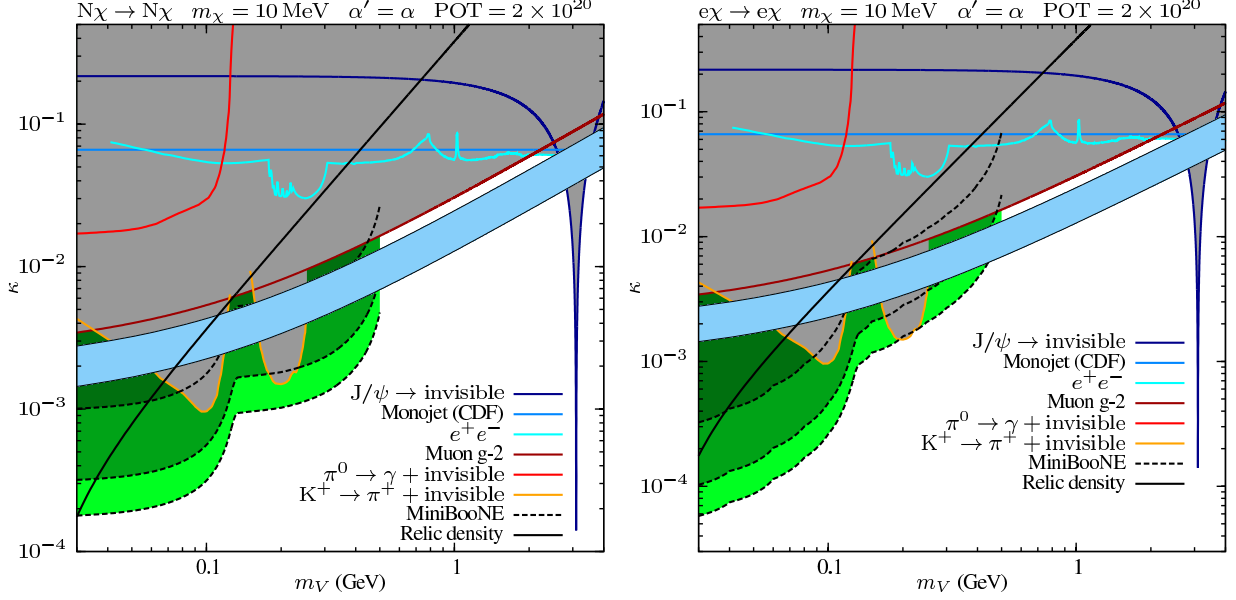


Figure 6: Regions of mixing angle κ vs vector mass m_V , showing the MiniBooNE sensitivity contours for the light dark matter scenario. The contours assume a WIMP mass $m_\chi = 10$ MeV and $\alpha' = \alpha$. The existing limits are as in Fig. 5, while the solid black line again shows the parameters required to reproduce the observed relic density of dark matter. The left panel shows regions where we expect 1–10 (light green), 10–1000 (green), and more than 1000 (dark green) elastic scattering events off nuclei in the MiniBooNE detector with 2×10^{20} POT. The right panel shows the same for elastic scattering off electrons. The green lobes showing enhanced sensitivity at lower mass are the result of vectors produced in π^0 decays while the right lobes show those from η decays. Note that for sufficiently low mass vectors, $m_V < \mathcal{O}(100 \text{ MeV})$ with $m_\chi \ll m_V/2$, the electron scattering search at LSND [38] will also impose constraints at the $\kappa \sim 10^{-3}$ level as discussed in [4].

sensitivity for the same POT, and is why this proposal is requesting running with the 25m absorber deployed.

WIMP production is via the vector mediator coupling to the photons in π^0 and η decay. In beam off target running, the protons interacting in the Fe target produce these neutral mesons, to first order, at the same rate as in Be. Furthermore, since they decay quickly ($\sim 10^{-16} \text{ sec}$) they are not absorbed and hence can still produce WIMPs. Thus, while neutrino production is severely reduced in beam dump mode, the production mechanism for WIMPs does not change. Also, it is obvious that WIMP production, if any, scales with protons on target.

4.2 WIMP Signal Extraction

Once produced in the beam, WIMPs can travel the ~ 500 m distance through rock to interact in the detector. The main interaction mode is neutral current (NC) like scattering off nucleons or electrons in the mineral oil (CH_2). To first order, WIMP scattering will look like neutrino neutral current scattering, though with different possible kinematics. MiniBooNE has already published results on NC nucleon scattering cross section, demonstrating that measurements of this type of process are possible [23]. Measurements of neutrino electron elastic scattering were performed and were reported in a thesis [39].

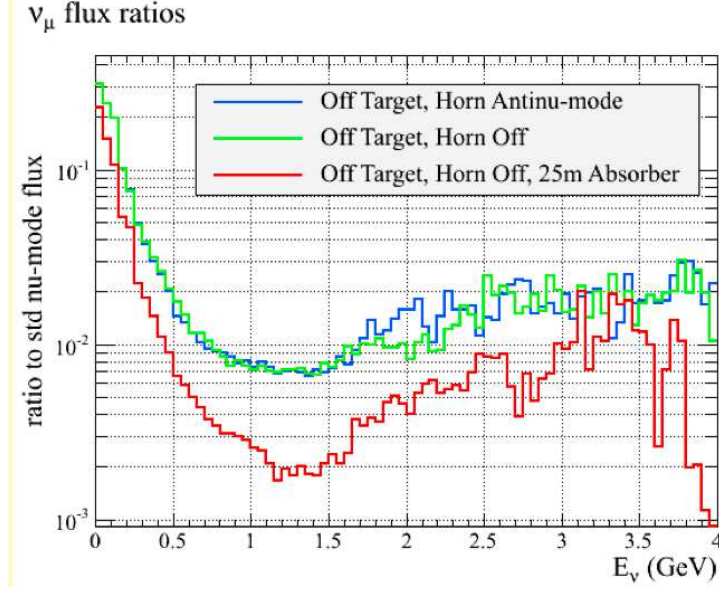


Figure 7: Neutrino flux reduction relative to normal neutrino mode as a function of neutrino energy for various modes.

In both cases, searching for WIMP like signals will have to contend with the dominant neutrino scattering background. Therefore, any technique that can significantly reduce this background will improve the sensitivity of the search. Two main methods will be employed: First, using the beam off target method coupled with simple counting or energy fits; Second, using event timing relative to the beam to look for sub-luminal WIMPs.

4.2.1 WIMP Sensitivities with NC Nucleon data set

MiniBooNE has already published a detailed analysis of the neutral current nucleon neutrino cross sections based on 6.5×10^{20} POT [23]. The reconstructed nucleon kinetic energy was required to be less than 650 MeV. The reconstruction efficiency is 35% and the NC nucleon purity 65%. The backgrounds came from various neutrino induced reactions such as neutrino interactions in the dirt, NC-like events, and others. There were a total of 95,531 NC events that were reconstructed. The total systematic error was estimated at 18.1%. There was no significant excess of events observed over the absolutely normalized Monte Carlo. Figure 9 shows the NC nucleon kinetic energy for data and Monte Carlo.

We can perform a simple counting experiment using the presently published 6.5×10^{20} POT NC elastic scattering analysis and assuming 18.1% systematic error. Given that no significant excess over background was observed, this gives a 90% C.L. upper limit of 22,136 events. The analysis for antineutrino mode NC nucleon cross sections is not yet published, but using preliminary estimates the number of reconstructed events for 10.1×10^{20} POT is 60,605 with 21% systematic errors. This corresponds to a 90% C.L. upper limit of 16,294 events assuming no excess of signal events.

Clearly, with the large number of backgrounds in normal beam on target mode, the limits are rather poor given the systematic errors at the $\sim 20\%$ level. The best way to improve

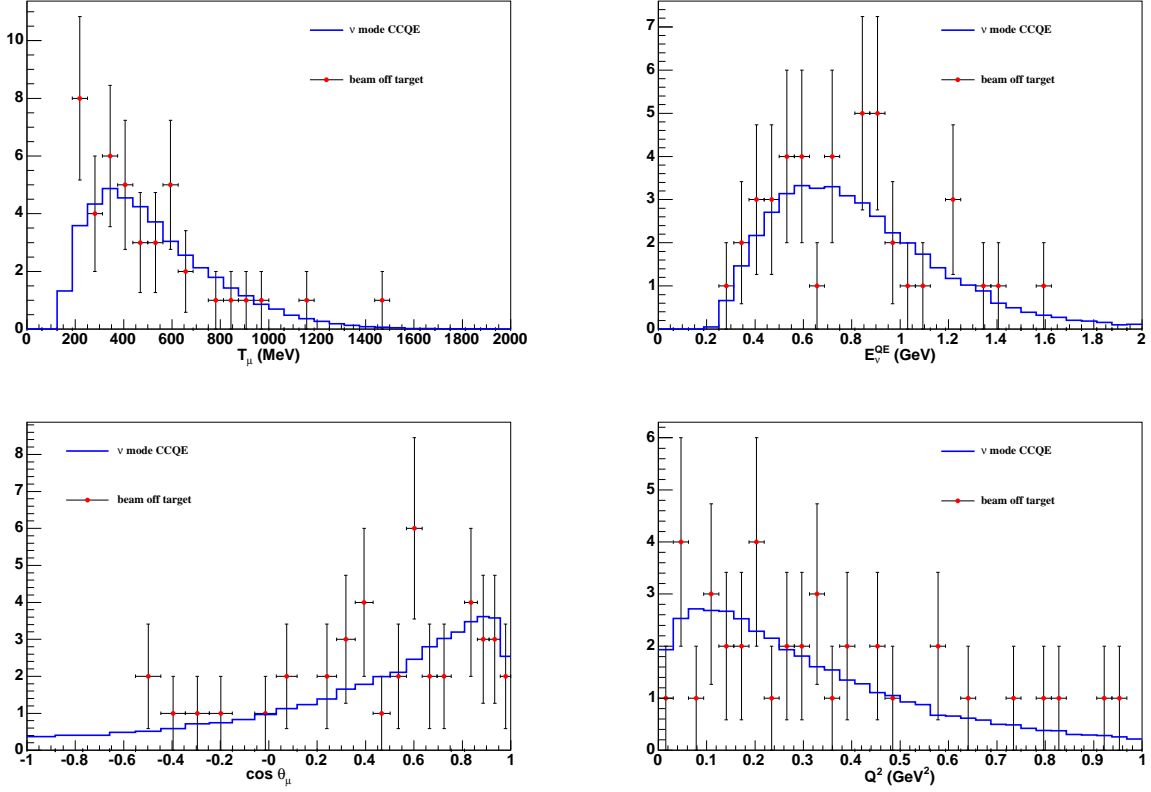


Figure 8: Reconstructed muon neutrino event kinematics (error bars) with the relatively normalized Monte Carlo overlaid (line). The data corresponds to the special 5.5×10^{18} POT beam off target run in March of 2012.

these limits is to reduce the backgrounds from neutrino interactions. If we run in beam off target mode with the 50m absorber, then we can reduce the neutrino induced NC events, and other backgrounds, by a factor of 42. For the equivalent 6.5×10^{20} POT, this corresponds to a data scaled prediction of 2,275 events and a 90% C.L. upper limit of 531 events assuming the same systematic errors. This is considered an upper limit because with the reduction in the neutrino flux and various backgrounds, signal cuts can be relaxed to increase efficiency and reduce errors. These improvements will be discussed in Section 4.4. Table 1 shows the expected sensitivities for a number of beam configurations based on a simple counting analysis. For the preferred case of 2.0×10^{20} POT and the 25m absorber, the neutrino backgrounds are reduced to only 350 events, with a 90% C.L. upper limit of 85 events. These projections are based on a simple counting analysis where we used the systematic error of 18.1% which was reported for the neutrino mode analysis. Besides using the 90% C.L. upper limits as a figure of merit, one needs to fold in the WIMP signal production that goes linearly with protons on target. This will be detailed in Section 4.3 where the final sensitivities are shown for 2.0×10^{20} POT.

A background that does not benefit from the beam off target reduction are beam uncorrelated events from cosmic rays. For the neutral current elastic analysis this background is

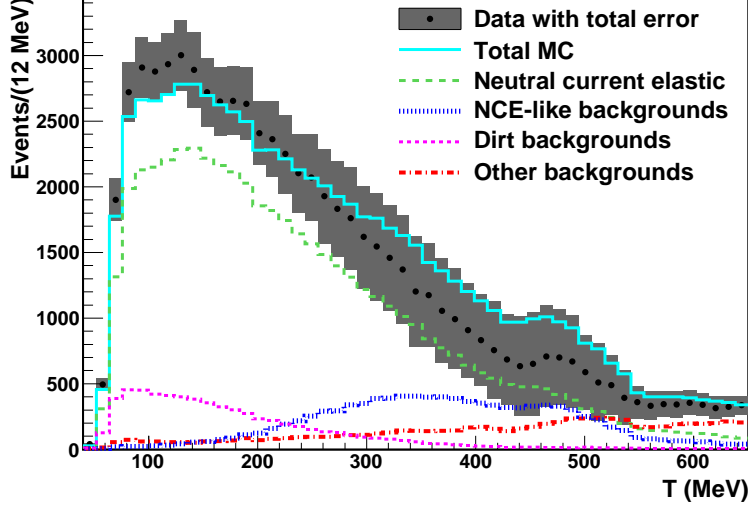


Figure 9: The NC nucleon event reconstruction for 6.5×10^{20} POT in neutrino mode [23]. The Monte Carlo is absolutely normalized.

estimated at 0.5%. Thus, for beam off target running with the 25m absorber and 2.0×10^{20} POT, this corresponds to 147 events, or about half the beam related backgrounds. However, these events can be measured to high accuracy due to the large number of random (strobe) triggers that are taken throughout the run. These events can be subtracted off with little systematic error. Finally, most of the subtraction occurs at kinetic energies above 400 MeV, which is above most of the signal region. Currently this error is not included in the sensitivity limits in Table 1, but is small and has almost no effect on the 90% C.L. upper limits since they are dominated by the systematic error on the neutrino backgrounds.

It is worth noting that if we do run with scintillator, as outlined in the submitted LOI, then the detection threshold for nucleons might be as low as 10 MeV. This will enhance the overall signal efficiency for WIMP detection since NC-like events tend to have an $1/E$ distribution, which pile up at low energy.

4.2.2 WIMP Sensitivities with NC Electron data set

In the case of elastic scattering off electrons, we can make use of the kinematic fact that WIMP scattering will put the electron in a very forward direction with respect to the beam direction. In fact, the scattering angle with respect to the beam, θ_{beam} , will mostly satisfy $\cos \theta_{beam} > 0.99$ for WIMP scattering as well for electroweak neutrino-electron scattering. This is observable given that the MiniBooNE direction reconstruction sensitivity is 3 degrees [40]. Figure 10 shows a plot of the Monte Carlo generated backgrounds in the $\cos \theta_{beam} > 0.90$ region for neutrino running. The strong peak at $\cos \theta_{beam} > 0.99$ is from neutrino-electron elastic scattering. This demonstrates MiniBooNE's ability to reconstruct this class of events, which kinematically resembles WIMP scattering off electrons. A simple cut $\cos \theta_{beam} > 0.99$ reduces neutrino backgrounds by 98%. A more sophisticated analysis will fit the backgrounds and then extrapolate into the region $\cos \theta_{beam} > 0.99$ to estimate the signal. This method has the advantage of not relying on the Monte Carlo for background estimations, and hence,

POT ($\times 10^{20}$)	Beam Configuration	25m Absorber ν -Background	25m Absorber 90% U.L.	50m Absorber ν -Background	50m Absorber 90% U.L.
10.1	$\bar{\nu}$ beam on target			60605	16294
6.5	ν beam on target			95531	22136
6.5	beam off target	1137	267	2275	531
4.0	beam off target	700	166	1400	328
2.0	beam off target	350	85	700	166
1.0	beam off target	175	44	350	85

Table 1: Estimated WIMP sensitivity 90% C.L. upper limits in the neutral current nucleon channel for various POT and absorber configurations. The top two rows are limits that can be set with the current neutrino and antineutrino data sets. The neutrino and beam off target mode systematic errors assumed are 18.1%, and for antineutrino mode 21%. Cosmic backgrounds are not included, but have only a small contribution to the 90% C.L. upper limits.

significantly reduces systematic errors.

For 6.5×10^{20} POT neutrino mode, and standard oscillation cuts, the predicted number of electron events from all sources of neutrino induced backgrounds for $\cos \theta_{beam} > 0.99$ is 41 events. This has an estimated 12% systematic error. Assuming no excess, this translates into 10.3 events at 90% C.L. upper limit. This is much better than the limit from the NC nucleon channel since we can rely on the forward scattering of the events to reject background. However, WIMP scattering off electrons is reduced in rate due to the reduced scattering cross sections. The combined effects of this will be shown in Section 4.3 on sensitivities. Table 2 shows predicted sensitivities for various POT and absorber configurations. For the preferred case of 2.0×10^{20} POT and the 25m absorber, the neutrino backgrounds are reduced to only 0.15 events, with a Poisson 90% C.L. upper limit of 2.5 events. In fact, for the various beam off target running options the 90% C.L. upper limits don't change much since backgrounds are reduced to such negligible levels. However, signal significance, if there is a signal, improves with reduced backgrounds, as discussed in Section 4.3

For the electron channel the beam uncorrelated backgrounds (cosmics) will not be a concern as the angle cut further constrains these events to negligible numbers of ~ 0.01 events for the standard oscillation cuts and 2.0×10^{20} POT. However, estimates of their rates will be measured with random triggers during the run to ensure this background is properly accounted.

4.2.3 Using Timing to Enhance Wimp Sensitivity

The WIMP mass region where MiniBooNE is sensitive is from 10 MeV up to about a 200 MeV (for various choices of model parameters). Given the ~ 500 m travel distance of the WIMPs from the production point to the detector, and the few nsec absolute timing resolution of the detector relative to the proton beam, we have the ability to separate out neutrino events that travel at the speed of light from WIMPs with masses above 50 MeV. This allows better signal to background rejection and improves detection sensitivities.

Figure 11 shows a simple drawing of WIMP production and detection relative to the

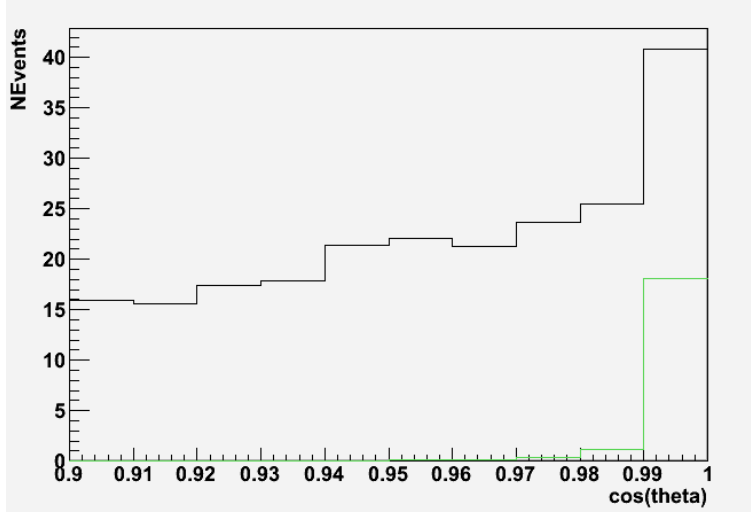


Figure 10: The Monte Carlo generated $\cos \theta_{beam}$ distribution for the electron data set with standard oscillation cuts. The black line is the total background, while the green line shows the contribution from elastic scattering off electrons.

POT ($\times 10^{20}$)	Beam Configuration	25m Absorber ν -Background	25m Absorber 90% U.L.	50m Absorber ν -Background	50m Absorber 90% U.L.
10.1	$\bar{\nu}$ beam on target			31	8.6
6.5	ν beam on target			41	10.3
6.5	beam off target	0.45	2.75	0.90	3.20
4.0	beam off target	0.30	2.60	0.60	2.90
2.0	beam off target	0.15	2.45	0.30	2.60
1.0	beam off target	0.08	2.38	0.15	2.45

Table 2: Estimated WIMP sensitivity 90% C.L. upper limits in the neutral current electron channel for various POT and absorber configurations. A systematic error of 12% was assumed. Cosmic backgrounds are not included, but have only small contribution to the 90% C.L. upper limits.

various experiment components. A key criteria is that protons range out in the iron absorber in $\sim 1\text{m}$ and the π^0 and η , which the WIMPs couple to, decay promptly on the order of 10^{-16} seconds. This localizes spatially and temporally the production point of the WIMPs. The produced WIMPs then travel to the detector at a velocity based on their mass and momentum. Figure 12 shows the relationship between WIMP mass and timing delay for an assumed momentum of 1.5 GeV, which is the mean momentum for typical production kinematics with the 8.9 GeV proton beam.

The absolute time of events reconstructed in the detector can be referenced to the beam resistive wall monitor (RWM) signal that records when the protons cross a point just a meter upstream from the target. The RWM signal is propagated via cable to the detector where the arrival time is recorded. Events are reconstructed and the timing of the event can be referenced to the RWM signal. Figure 13 shows a plot of the reconstructed CCQE muon timing relative to the RWM signal. Events on either side of the Gaussian centroid can be

Timing cut (nsec)	Background Reduction (%)	WIMP Velocity β	WIMP Mass (MeV)
3.0	90	0.9984	85
4.6	99	0.9974	108
5.9	99.9	0.9967	122

Table 3: WIMP velocity for various WIMP masses, assuming a WIMP momentum of 1.5 GeV. Also shown are the timing delay (cut) and background reduction levels achieved for a specific WIMP velocity.

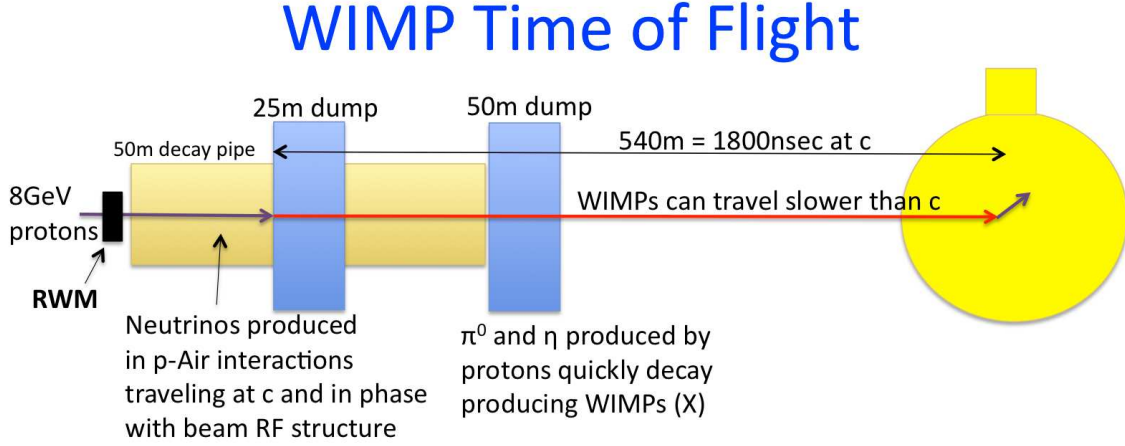


Figure 11: Simple timing drawing showing the production and reconstruction of events.

considered out of time, i.e. these are events that fall within the 53 MHz buckets, and are out of time either early or late, though we will assume they are late for this analysis.

Preliminary studies indicates that the time resolution achievable is ~ 1.8 nsec. Thus to reach 99% in-time event rejection, requires a time cut at 4.6 nsec. This corresponds to a WIMP mass threshold of 108 MeV assuming a WIMP momentum of 1.5 GeV. The 4.6nsec cut would also reject about 50% of the signal events as well. Table 3 shows the results for other rejection levels. Of course this is a simple illustrative analysis where we pick a single threshold cut. The real analysis would involve fits to the timing distribution to extract any possible signal above the background levels.

The sensitivities shown in Section 4.3 involve a simple threshold model as a function of β where the sensitivity change can be incorporated into the limits. It is evident that the use of absolute event timing will significantly enhance the sensitivity for WIMP searches at the higher end of the MiniBooNE mass sensitivity.

One complication to the analysis is that the RWM corrected timing distribution is not quite Gaussian. This is due to kaons produced by the beam that travel slower than c which then decay to neutrinos that will have a slight time delay relative to the majority of neutrinos produced by pion decay. Monte Carlo studies show that 90% of these events have a time delay of less than 4 nsec. The remaining events that extend into the Gaussian tail can be measured using the high statistics timing data sample from the neutrino run. For the beam off target running with the 25m absorber and 2.0×10^{20} POT, the number of nucleon scattering events with timing > 4 nsec is estimated to be only a few events.

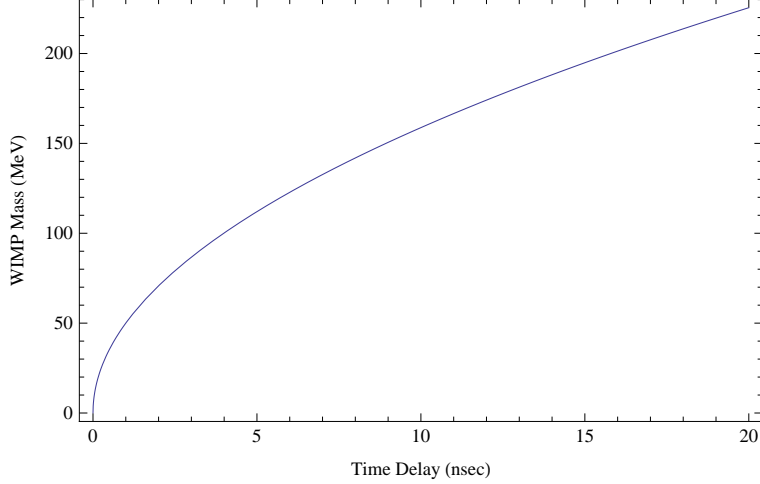


Figure 12: WIMP mass versus time delay for an assumed WIMP momentum of 1.5 GeV.

4.3 Sensitivity Plots and Signal Significance

Putting together the counting limits with timing information, the following plots show the MiniBooNE event sensitivities. Figure 14 shows the WIMP-nucleon scattering sensitivities and Figure 15 shows the WIMP-electron scattering sensitivities. All sets of plots are for the requested 2.0×10^{20} POT. These plots show the predicted MinibooNE counting sensitivities for the 25m and 50m absorber modes.

Clearly the beam off target modes enhance the sensitivity and reach by about an order of magnitude lower in cross section into unexplored regions of parameter space. Importantly, it covers the region of the muon g-2 signal, up to the limit of MiniBooNE mass sensitivity which is about 200 MeV and which is a little less than half the η mass (near mass threshold the sensitivities fall off). The left plots shown here are for a vector mediator mass $M_V = 300$ MeV, the right plots for $M_X = 10$ MeV, and both plots for $\alpha' = \alpha$. The choice of these parameters are discussed in the Section 3.2.

It is clear that the 25m absorber option is preferred as it covers more parameter space in the nucleon scattering channel. For the case of electrons, in all cases, we reach the Poisson 90% C.L. sensitivity of 2.3 events. However, with the extra flux reduction achieved with the 25m absorber we will be able to loosen the particle identification cuts enough to increase the electron reconstruction efficiency. This is equivalent to adding more protons on target.

Besides sensitivity limits, the other consideration is the significance of any possible signals. Table 4 shows the calculated signal significance for four solution points along the central muon g-2 signal band, as shown in Figure 16. It is apparent that along the muon g-2 band MiniBooNE has good signal significance. Solution three is interesting as it is the crossing point of muon g-2, relic density and MiniBooNE. Clearly we can probe this interesting point with high significance.

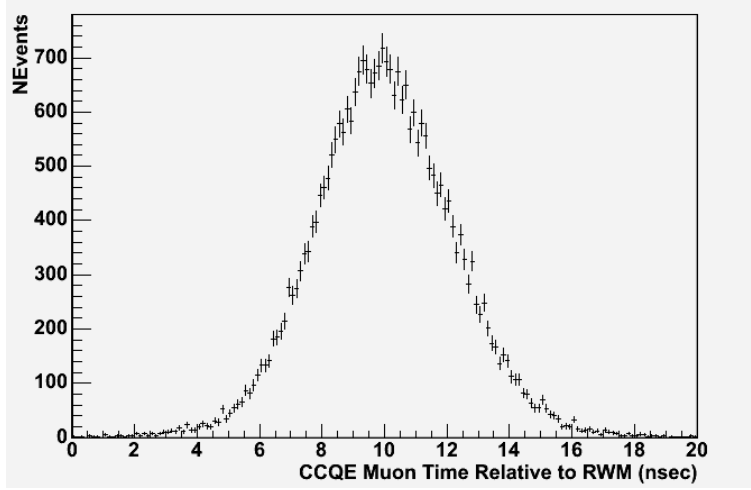


Figure 13: Absolute muon CCQE event timing relative to the RWM beam signal. The timing RMS of the Gaussian is approximately 1.8 nsec.

	Scattering Channel	Beam Mode (2.0×10^{20} POT)	WIMP mass (MeV)/ cross section (cm^2)	Signal	Background and Errors	Probability
1	Nucleon	25m	$10/4 \times 10^{-37}$	1859	350 ± 66	$< 10^{-10}$
2	Nucleon	25m	$30/3 \times 10^{-36}$	1453	350 ± 66	$< 10^{-10}$
3	Nucleon	25m	$50/8 \times 10^{-36}$	1326	203 ± 40	$< 10^{-10}$
4	Nucleon	25m	$100/3 \times 10^{-35}$	1186	9.2 ± 3.4	$< 10^{-10}$
1	Electron	25m	$10/4 \times 10^{-37}$	13.2	0.15	$< 10^{-10}$
2	Electron	25m	$30/3 \times 10^{-36}$	7.7	0.15	$\sim 10^{-9}$
3	Electron	25m	$50/8 \times 10^{-36}$	4.8	0.09	$\sim 10^{-6}$
4	Electron	25m	$100/3 \times 10^{-35}$	1.4	0.004	$\sim 10^{-3}$

Table 4: Signal significance (probability of background fluctuating up to the signal level) for various points in WIMP mass and cross section parameter space for nucleon and electron channel (see Figure 16). The reduction in backgrounds at higher WIMP mass are due to the timing cuts increasing effectiveness. Assumed vector mediator mass $M_V = 300$ MeV.

4.4 Analysis Improvements

The kinetic energy of the nucleons and electrons from WIMP scattering will depend on the kinematics of the WIMP production and the scattering kinematics in the detector. This is somewhat model dependent and should be included in fits. If there are differences from the kinetic energy of the background, then the use of energy will improve the significance and help determine the model parameters (m_χ , m_V , κ , and α'). In order to do this the model needs to be incorporated into the MiniBooNE Monte Carlo code, which will be a future analysis project. Without the Monte Carlo events from the model in hand, it is currently hard to predict if there will be any benefit from using kinetic energy information. This will be carefully studied.

Another avenue for improvement is to increase the signal efficiency of the reconstructed nucleons and electrons. With a current reconstruction efficiency of 35% for nucleons and

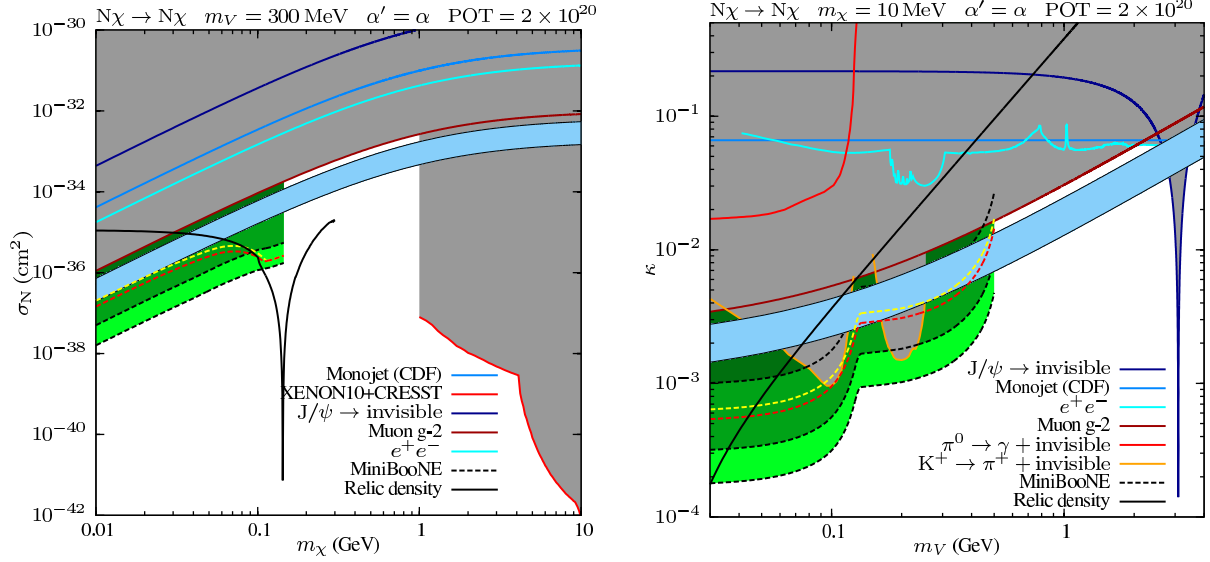


Figure 14: The cross section versus WIMP (left) and vector mediator (right) mass for the nucleon scattering channel for 2.0×10^{20} POT. MiniBooNE estimated 90% C.L. upper limits for 50m absorber (dashed yellow), and 25m absorber (dashed red) are shown. The left plot assumes a mediator mass $M_V = 300$ MeV, and the right plot assumes a WIMP mass $M_X = 10$ MeV.

15% for electrons, there is some room for improvement. The electron channel would gain the most from such an improvement.

In beam off target running there is a large neutrino background reduction, therefore one can explore the possibility of looser particle identification (PID) cuts to enhance signal efficiency. This is especially true for the electron channel where there is a huge reduction in background from both beam off target flux reduction, $\cos \theta_{beam}$, and timing cuts. With such a large background reduction, a factor of two improvement in the electron efficiency is very likely. The simplest way is to loosen some of the geometrical cuts necessary to reduce neutrino induced dirt backgrounds coming from outside the detector. Also, with the large π^0 background reduction, the electron- π^0 likelihood can be loosened. This cut reduces the electron efficiency the most in the regular oscillation analysis, which is required to reduce this large and insidious background. With the $\cos \theta_{beam}$ requirement this background becomes less problematic, and is well measured outside the signal region. Initial estimates is that we will be able to double the electron efficiency. For the case of nucleon scattering we might be able to make some improvements in efficiency, but it won't be as dramatic as for the electron case.

Even if none of these possible improvements bear fruit, the basic proposal here will succeed with the current analysis techniques developed for the oscillation and NC nucleon analysis.

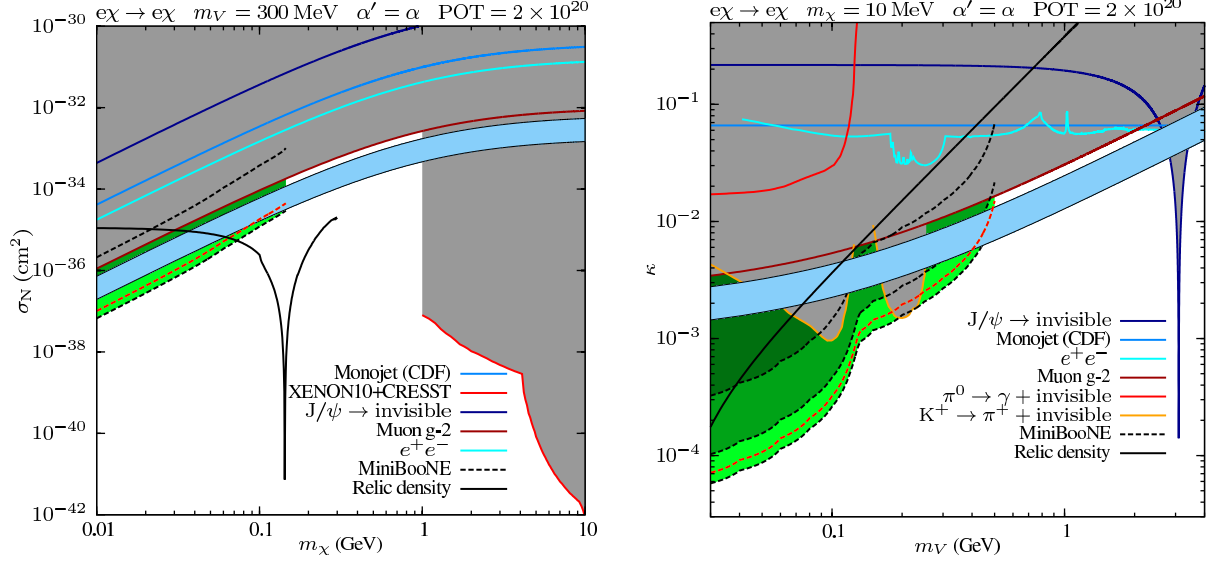


Figure 15: The cross section versus WIMP (left) and vector mediator (right) mass for the electron scattering channel for 2.0×10^{20} POT. MiniBooNE estimated 90% C.L. upper limits for 50m absorber (dashed yellow), and 25m absorber (dashed red) are shown (here the red overlays the yellow dashed lines). The left plot assumes a mediator mass $M_V = 300$ MeV, and the right plot assumes a WIMP mass $M_\chi = 10$ MeV.

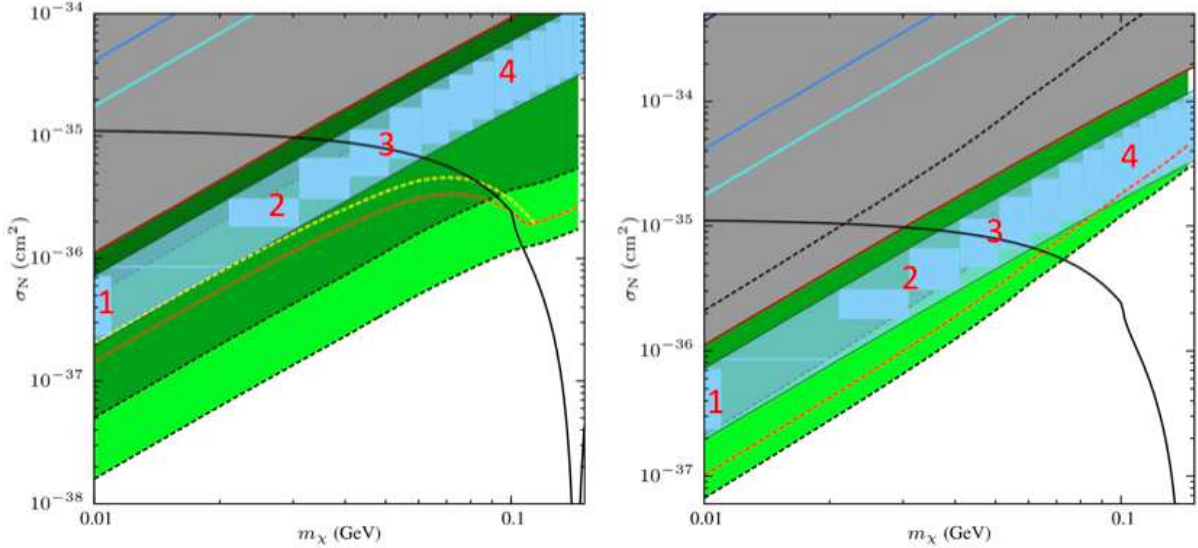


Figure 16: A zoomed in look at the MiniBooNE sensitivity for WIMP-nucleon (left) and WIMP-electron (right) scattering channels. Overlaid are the four signal points considered in Table 4. The plots are for a mediator mass $M_V = 300$ MeV and 2.0×10^{20} POT.

5 Timing and Beam Targeting Improvements

It was reported in Section 4.2.3 that the timing resolution achieved was 1.8 nsec. This is true for neutrino mode running; in antineutrino mode it was found to be about 2.2 nsec. This was due to the requirement that muon neutrino events be used to calibrate timing offsets to account for changes in the various timing components. In antineutrino mode, the event rate is five times lower, and hence the data available for calibration is reduced and the time between events is longer, diluting the effectiveness of the calibrations. As well, the antineutrino RWM timing hardware was compromised for about 40% of the run and cannot be used for the timing analysis.

Finally, cuts were required in both neutrino and antineutrino mode to remove various timing instabilities in the circuit. Much of this was caused by the fact that the transmission cable between the RWM in the target and the detector is via a copper coaxial cable. This is susceptible to lightning strikes causing electronics to be burned out and adding instability to the data. Many of these effects have been mitigated, but still cause some concern and bias in the analysis.

We are presently installing a new fiber timing circuit that will have better inherent timing stability and will not be susceptible to lightning effects. We expect a major improvement in the analysis to the point where we will not have to rely on the muon neutrino data to calibrate the timing offsets. This is especially important for beam off target running where there will be minimal muon neutrino data for timing calibration. We will also be installing a digitizer (as a new ACNET device) that will record the RWM signal, thus recording a detailed trace of the beam RF structure for each beam spill. This will add information on the beam structure available to the timing analysis on an event by event basis.

Another improvement will be the installation of new dual low mass multiwires in the beamline at position 875 just a few meters upstream from the target. The two multiwires are separated by 1m. With a 0.25mm spatial resolution, we will be able to point the proton beam within 0.5 mradian angle resolution. This means we can project the direction of the beam to within about 25cm in the detector. This is important if we are going to search for physics effects correlated with the beam direction.

6 Deploying the 25m Absorber

Besides the physics improvements of the 25m absorber over the 50m, there is also the advantage that the 25m absorber is a single block of iron 12' x 12' on its sides and 18" long. There are 11 blocks (one of which is concrete) which make up the whole absorber length. The 50m absorber contains many blocks that are stacked on top of each other. The transverse face to the beam has many cracks and gaps. Though unlikely, the proton beam could be striking one of these cracks, compromising our understanding of the meson production and absorption. With the 25m absorber one knows the proton beam is fully striking the iron and producing neutral mesons at one localized position.

Estimates from Accelerator Division put the cost of deploying the 25m absorber at \$80k and requires 2.5 weeks. A significant fraction of the cost is the required large crane to lower the blocks in place. Given that six years ago we accessed the 25m absorber to replace all the

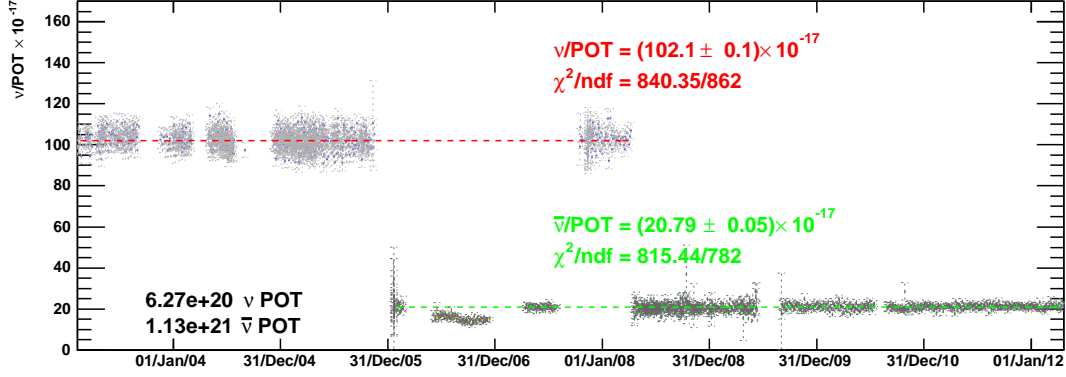


Figure 17: The neutrino per POT for the entire MiniBooNE run. The antineutrino/POT rate is down by a factor of five due to the reduced flux and cross sections. The antineutrino χ^2/DF does not include the period of fallen absorbers (May 06 to October 06), but that data is included in the oscillation analysis.

hanging chains with robust stainless steel rods, we feel this estimate is reliable. Of course, if MicroBooNE will run with the 50m absorber, then we will have to raise it, which will double the overall cost to \$160k and 5 weeks of beamline downtime.

7 Logistics of the Extended Run

MiniBooNE has been running well over the last ten years. Figure 17 shows the neutrino/POT for most of the run period. As can be seen, the overall beam stability is very good. Besides changing out the horn in 2004 and the period of the fallen 25m absorber in early 2006, running has been very smooth. Figure 18 shows the reconstructed muon neutrino energy over the last six years of MiniBooNE antineutrino running, which demonstrates the detector response and energy scale stability. This is critical for good reconstruction and particle identification, and again shows overall excellent performance and stability of the horn, oil, PMTs, and electronics. The overall stability of the experiment is crucial for continued running. This has been achieved in the past, and should continue into the future. The above distributions are just some of the monitoring inputs that are reviewed on a regular basis.

The success of the run requires a minimum number of personnel to staff shifts on a continual basis. A two year projection (2013 and 2014) of personnel available for running shifts, based on replies of collaboration members, is shown in Table 5. With a collaboration hire of a full time owl shifter, and the number of remaining collaborators, there are sufficient personnel available to staff shifts and experts on-site to handle run problems. With about 28 collaborators currently signed up, and a full time hire, the shift burden will be about 3 shifts a month. Given that the run is only about a year, and the high interest in the run itself, this is not considered too much of a burden. Furthermore, remote shifting was enabled four years ago that allows shifters to take shifts from remote institutions. This has been instrumental in allowing off-site personnel to continue shift duties and participation in the experiment.

The collaboration is open to allowing new institutions/collaborators to join. Already we have the addition of theory collaborators from the University of Chicago and the University

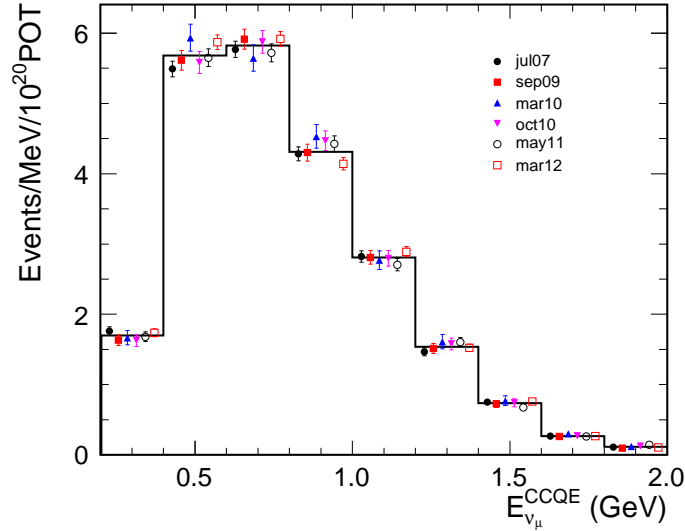


Figure 18: Energy scale calibrated with muon neutrino CCQE events. The neutrino production and detector response remain constant over the last six years.

of Victoria, though they are currently not added to the shifter pool. With a commitment to more running, the task of bringing aboard new collaborators would become an easier task to undertake.

Year	Number of Collaborators	New postdocs and students	Hired Full Tme Shifter
2007	54	0	0
2008	54	1	0
2009	54	1	1
2010	42	2	1
2011	42	0	1
2012	42	1	1
2013	28	unknown	1
2014	28	unknown	1

Table 5: *Projected MiniBooNE shift personnel. 2013 and 2014 is projected based on collaborators willingness to continue on MiniBooNE. We began remote shifting in 2009, which has been instrumental in reducing the constant shift burden. The FTE equivalent is about 50% and the full time shifter staffs 25% of all shifts.*

With the analysis in place from both the ν_e and the $\bar{\nu}_e$ appearance results, the addition of the extra beam off target data is straight forward and, as a minimum, will only require reprocessing the data and extra Monte Carlo simulations. There are sufficient computer resources and personnel to perform the analysis successfully. Given the interest in the topic of WIMP searches, we will find a student to perform the analysis in conjunction with the addition of at least one new postdoc that has been hired. As a minimum, we are guaranteed to publish one to two papers on WIMP limits, or signals.

The beamline, horn system, and detector have been operating well for the duration of the experiment since 2002. One horn replacement has been needed, and a repair of the 25m absorber, but no major detector repairs or downtimes have occurred. A third horn and target are ready, as are spare accelerator parts, and spare detector electronics sufficient to run the experiment for at least one more year.

8 Summary

MiniBooNE has a unique opportunity to search for light mass WIMPs in the mass range from 10 MeV up to 200 MeV. The reach in cross section overlaps the muon $g - 2$ discrepancy when interpreted via coupling to a vector mediator V_μ . This sensitivity is achieved by running the beam past the target and impacting the 25m absorber, where neutrino production is severely reduced, subsequently reducing the neutrino background rate and enhancing searches for WIMPs, or other exotic physics. It should be noted that this proposal detailed a particular dark matter model to discuss concrete sensitivity. With such a large number of protons on target and a large electromagnetically sensitive detector, running in beam off target mode will be extremely sensitive to a number of other models that include axions, para-photons, dark photons, etc.

MiniBooNE is in a position to do this analysis in a timely manner as all the necessary particle identification tools have already been developed. We have studied the detector response over the last ten years and have published a number of neutrino oscillation and cross section measurements relevant for the present analysis.

MiniBooNE has a proven track record of delivering on its goals, both operationally and with publications. For minimal cost and only a one year run to collect 2.0×10^{20} POT, we can achieve relevant WIMP limits, or possibly a signal.

9 The Request

MiniBooNE requests running to collect a total of 2.0×10^{20} POT in beam off target mode and with the 25m absorber deployed. This will allow a powerful search for low mass WIMPs in a parameter region consistent with the required cosmic relic density, and in which these models can resolve the muon $g - 2$ discrepancy. The experiment further requests that this beam be delivered in FY2013 and 2014 before the MicroBooNE experiment turns on.

References

- [1] C. Athanassopoulos *et al.*, Phys. Rev. Lett. **75**, 2650 (1995); **77**, 3082 (1996); **81**, 1774 (1998); Phys. Rev. C. **58**, 2489 (1998); A. Aguilar *et al.*, Phys. Rev. D **64**, 112007 (2001).
- [2] A. A. Aguilar-Arevalo *et al.* [MiniBooNE Collaboration], arXiv:1207.4809 [hep-ex].
- [3] B. Batell, M. Pospelov and A. Ritz, Phys. Rev. D **80**, 095024 (2009) [arXiv:0906.5614 [hep-ph]].
- [4] P. deNiverville, M. Pospelov and A. Ritz, Phys. Rev. D **84**, 075020 (2011) [arXiv:1107.4580 [hep-ph]].
- [5] P. deNiverville, D. McKeen and A. Ritz, Phys. Rev. D **86**, 035022 (2012) [arXiv:1205.3499 [hep-ph]].
- [6] J. Goodman, M. Ibe, A. Rajaraman, W. Shepherd, T.M. Tait, et al., Phys. Rev. D **82**, 116010 (2010), [arXiv:1008.1783 [hep-ph]]; P.J. Fox, R. Harnik, J. Kopp, and Y. Tsai, Phys. Rev. D **84**, 014028 (2011), [arXiv:1103.0240 [hep-ph]]; A. Rajaraman, W. Shepherd, T. M. Tait, and A.M. Wijangco, Phys. Rev. D **84**, 095013 (2011), [arXiv:1108.1196 [hep-ph]]; P.J. Fox, R. Harnik, J. Kopp, and Y. Tsai, Phys. Rev. D **85**, 056011 (2012), [arXiv:1109.4398 [hep-ph]]; I.M. Shoemaker and L. Vecchi, (2011), arXiv:1112.5457 [hep-ph].
- [7] R. Essig, J. Mardon, and T. Volansky, (2011), arXiv:1108.5383 [hep-ph]; P.W. Graham, D.E. Kaplan, S. Rajendran, and M.T. Walters, (2012), arXiv:1203.2531 [hep-ph].
- [8] Y. Kahn and J. Thaler, arXiv:1209.0777 [hep-ph];
B. Wojtsekhowski, D. Nikolenko and I. Rachek, arXiv:1207.5089 [hep-ex].
- [9] C. Boehm, D. Hooper, J. Silk, M. Casse and J. Paul, Phys. Rev. Lett. **92**, 101301 (2004) [astro-ph/0309686].
- [10] N. Prantzos, C. Boehm, A. M. Bykov, R. Diehl, K. Ferriere, N. Guessoum, P. Jean and J. Knoedlseder *et al.*, arXiv:1009.4620 [astro-ph.HE].
- [11] B. W. Lee and S. Weinberg, Phys. Rev. Lett. **39**, 165 (1977).
- [12] C. Boehm and P. Fayet, Nucl. Phys. B **683**, 219 (2004) [hep-ph/0305261].
- [13] P. Fayet, Phys. Rev. D **70**, 023514 (2004) [hep-ph/0403226]
- [14] M. Pospelov, A. Ritz and M. B. Voloshin, Phys. Lett. B **662**, 53 (2008) [arXiv:0711.4866 [hep-ph]].
- [15] P. Gondolo and G. Gelmini, Phys. Rev. D **71**, 123520 (2005), [arXiv:hep-ph/0504010 [hep-ph]]; D.P. Finkbeiner and N. Weiner, Phys. Rev. D **76**, 083519 (2007), [arXiv:astro-ph/0702587 [astro-ph]]; D. Hooper and K.M. Zurek, Phys. Rev. D **77**, 087302 (2008), [arXiv:0801.3686 [hep-ph]]; N. Arkani-Hamed, D.P. Finkbeiner, T.R. Slatyer, and N. Weiner, Phys. Rev. D **79**, 015014 (2009), [arXiv:0810.0713 [hep-ph]]; M. Pospelov and A. Ritz, Phys. Lett. B **671**, 391 (2009), [arXiv:0810.1502 [hep-ph]].
- [16] P. Fayet, Phys. Rev. D **75**, 115017 (2007) [hep-ph/0702176 [HEP-PH]].
- [17] M. Pospelov, Phys. Rev. D **80**, 095002 (2009) [arXiv:0811.1030 [hep-ph]].
- [18] B. Batell, M. Pospelov, and A. Ritz, Phys. Rev. D **79**, 115008 (2009), [arXiv:0903.0363 [hep-ph]]; R. Essig, P. Schuster, and N. Toro, Phys. Rev. D **80**, 015003 (2009), [arXiv:0903.3941 [hep-ph]]; M. Reece and L.-T. Wang, JHEP **0907**, 051 (2009), [arXiv:0904.1743 [hep-ph]]; J.D. Bjorken, R. Essig, P. Schuster, and N. Toro, Phys. Rev. D **80**, 075018 (2009), [arXiv:0906.0580 [hep-ph]]; P. Schuster, N. Toro, and I. Yavin, Phys. Rev. D **81**, 016002 (2010), [arXiv:0910.1602 [hep-ph]]; R. Essig, P. Schuster, N. Toro, and B. Wojtsekhowski, JHEP **1102**, 009 (2011), [arXiv:1001.2557 [hep-ph]]; R. Essig, R. Harnik, J. Kaplan,

- and N. Toro, Phys. Rev. D **82**, 113008 (2010), [arXiv:1008.0636 [hep-ph]]; J. P. Lees *et al.* [BABAR Collaboration], Phys. Rev. Lett. **108**, 211801 (2012) [arXiv:1202.1313 [hep-ex]].
- [19] V. Barger, C. -W. Chiang, W. -Y. Keung and D. Marfatia, Phys. Rev. Lett. **106**, 153001 (2011) [arXiv:1011.3519 [hep-ph]]; D. Tucker-Smith and I. Yavin, Phys. Rev. D **83**, 101702 (2011) [arXiv:1011.4922 [hep-ph]]; B. Batell, D. McKeen and M. Pospelov, Phys. Rev. Lett. **107**, 011803 (2011) [arXiv:1103.0721 [hep-ph]].
 - [20] J. L. Hewett, H. Weerts, R. Brock, J. N. Butler, B. C. K. Casey, J. Collar, A. de Gouvea and R. Essig *et al.*, arXiv:1205.2671 [hep-ex].
 - [21] A.A. Aguilar-Arevalo *et al.*, Phys. Rev. D **83**, 052009 (2011).
 - [22] A.A. Aguilar-Arevalo *et al.*, Phys. Rev. D **83**, 052007 (2011).
 - [23] A.A. Aguilar-Arevalo *et al.*, Phys. Rev. D **82**, 092005 (2010).
 - [24] A.A. Aguilar-Arevalo *et al.*, Phys. Rev. D **81**, 092005 (2010).
 - [25] A.A. Aguilar-Arevalo *et al.*, Phys. Rev. D **81**, 013005 (2010).
 - [26] A.A. Aguilar-Arevalo *et al.*, Phys. Rev. Lett. **103**, 081801 (2009).
 - [27] A.A. Aguilar-Arevalo *et al.*, Phys. Lett. B **664**, 41 (2008).
 - [28] A.A. Aguilar-Arevalo *et al.*, Phys. Rev. Lett. **100**, 032301 (2008).
 - [29] B. Holdom, Phys. Lett. B **166**, 196 (1986).
 - [30] A. A. Aguilar-Arevalo *et al.* [MiniBooNE Collaboration], Phys. Rev. D **79**, 072002 (2009) [arXiv:0806.1449 [hep-ex]].
 - [31] G. Angloher, S. Cooper, R. Keeling, H. Kraus, J. Marchese, Y. A. Ramachers, M. Bruckmayer and C. Cozzini *et al.*, Astropart. Phys. **18**, 43 (2002).
 - [32] J. Angle *et al.* [XENON10 Collaboration], Phys. Rev. Lett. **107**, 051301 (2011) [arXiv:1104.3088 [astro-ph.CO]].
 - [33] I. M. Shoemaker and L. Vecchi, Phys. Rev. D **86**, 015023 (2012) [arXiv:1112.5457 [hep-ph]].
 - [34] M. Ablikim *et al.* [BES Collaboration], Phys. Rev. Lett. **100**, 192001 (2008) [arXiv:0710.0039 [hep-ex]].
 - [35] J. Barreto *et al.* [DAMIC Collaboration], Phys. Lett. B **711**, 264 (2012) [arXiv:1105.5191 [astro-ph.IM]].
 - [36] M. S. Atiya, I. H. Chiang, J. S. Frank, J. S. Haggerty, M. M. Ito, T. F. Kycia, K. K. Li and L. S. Lit-tenberg *et al.*, Phys. Rev. Lett. **69**, 733 (1992).
 - [37] A. V. Artamonov *et al.* [E949 Collaboration], Phys. Rev. Lett. **101**, 191802 (2008) [arXiv:0808.2459 [hep-ex]].
 - [38] L. B. Auerbach *et al.* [LSND Collaboration], Phys. Rev. D **63**, 112001 (2001) [hep-ex/0101039].
 - [39] S.A. Ouedraogo, "Limit on the Muon Neutrino Magnetic Moment and a Measurement of the CCPIP to CCQE Cross-Section Ratio", PhD Thesis, Louisiana State University, 2008
 - [40] R. B. Patterson, E. M. Laird, Y. Liu, P. D. Meyers, I. Stancu and H. A. Tanaka, Nucl. Instrum. Meth. A **608**, 206 (2009) [arXiv:0902.2222 [hep-ex]].